STEM CELLS
TRANSLATIONAL MEDICINE

Mesenchymal stem cells and three-dimensional-osteoconductive scaffold regenerate calvarial bone in critical size defects in swine

Zoe M. Johnson[1] 🔬 | Yuan Yuan[1] | Xiangjia Li[2,3] | Tea Jashashvili[4] | Michael Jamieson[5] | Mark Urata[6] | Yong Chen[3] | Yang Chai[1] 🔬

[1]Center for Craniofacial Molecular Biology, Herman Ostrow School of Dentistry, University of Southern California, Los Angeles, California

[2]Department of Aerospace and Mechanical Engineering, School for Engineering of Matter, Transport and Energy, Arizona State University, Tempe, Arizona

[3]Viterbi School of Engineering, University of Southern California, Los Angeles, California

[4]Molecular Imaging Core, University of Southern California, Los Angeles, California

[5]Ottawa Hospital Research Institute, Ottawa, Canada

[6]Division of Plastic and Maxillofacial Surgery, Children's Hospital Los Angeles, Los Angeles, California

Correspondence
Yang Chai, DDS, PhD, George and MaryLou Boone Chair in Craniofacial Biology, Center for Craniofacial Molecular Biology, University of Southern California, 2250 Alcazar Street—CSA 103, Los Angeles, CA 90033, USA.
Email: ychai@usc.edu

Funding information
Alfred Mann Institute (AMI) at the University of Southern California; National Institute of Dental and Craniofacial Research National Institute of Health—Center for Dental, Oral and Craniofacial Tissue and Organ Regeneration (C-DOCTOR), Grant/Award Numbers: U24 DE029463, U24 DE026914

Abstract

Craniofacial bones protect vital organs, perform important physiological functions, and shape facial identity. Critical-size defects (CSDs) in calvarial bones, which will not heal spontaneously, are caused by trauma, congenital defects, or tumor resections. They pose a great challenge for patients and physicians, and significantly compromise quality of life. Currently, calvarial CSDs are treated either by allogenic or autologous grafts, metal or other synthetic plates that are associated with considerable complications. While previous studies have explored tissue regeneration for calvarial defects, most have been done in small animal models with limited translational value. Here we define a swine calvarial CSD model and show a novel approach to regenerate high-quality bone in these defects by combining mesenchymal stem cells (MSCs) with a three-dimensional (3D)-printed osteoconductive HA/TCP scaffold. Specifically, we have compared the performance of dental pulp neural crest MSCs (DPNCCs) to bone marrow aspirate (BMA) combined with a 3D-printed HA/TCP scaffold to regenerate bone in a calvarial CSD (>7.0 cm^2). Both DPNCCs and BMA loaded onto the 3D-printed osteoconductive scaffold support the regeneration of calvarial bone with density, compression strength, and trabecular structures similar to native bone. Our study demonstrates a novel application of an original scaffold design combined with DPNCCs or BMA to support regeneration of high-quality bone in a newly defined and clinically relevant swine calvarial CSD model. This discovery may have important impact on bone regeneration beyond the craniofacial region and will ultimately benefit patients who suffer from debilitating CSDs.

KEYWORDS
bone marrow aspirate, critical size defect, dental pulp neural crest cell, hydroxyapatite tricalcium phosphate, mesenchymal stem cells

1 | INTRODUCTION

Craniofacial bones protect vital organs, contribute to our facial identity, and serve as our interface with the world. They can also affect the way we sense our environment, eat, and communicate with others. Damage to these bones is detrimental not only to the function of these structures, including their crucial protection of the brain, but also to the psychosocial well-being of the patient, as it can quite literally change the face that is presented to the world. There are a multitude of causes of craniofacial bone defects and many approaches to repairing them.[1,2]

Due to an increase in the overall survival of neurotraumatic events such as open skull trauma, stroke, and subarachnoid hemorrhage necessitating decompressive craniectomy, the number of cranioplasties performed in the United States now exceeds 5000 each year.[3] Incidents of head trauma, congenital defects, disease, and tumor resection often leave patients with large, full-thickness calvarial defects that are incapable of healing on their own.[4] These critical-size defects (CSDs) are typically filled by surgeons using metal or other synthetic implants, which are inconvenient for the patient, associated with significant morbidity and potential infection, and inferior architecturally to natural bone.[5] In pediatric patients, these implants fail to accommodate postnatal brain growth.[4] Furthermore, resorbable plates have tensile strength only for 3-4 weeks but often take longer than a year to resorb, decreasing opportunities for a more natural interface with existing bone to develop.[6] Only biological materials can participate in such a process of growth and feedback. Autologous bone grafting is another solution.[7] However, for injuries of critical size, there may not be enough autologous bone elsewhere in the body suitable for grafting. Bone transplantation also often results in tissue rejection or, particularly in pediatric patients, in resorption.[8] Bone grafting also causes additional trauma to the body which should be avoided if possible. Current solutions for craniofacial CSDs are thus unsatisfactory and there is a significant clinical need for improved treatment modalities.

Recently, mesenchymal stem cells (MSCs) have shown great promise in injury repair studies due to their ability to differentiate into osteoblasts, chondrocytes, adipocytes, myocytes, neuron-like cells, and other cell types.[9] MSCs can proliferate as undifferentiated stem cells and later be guided to differentiate into the desired lineage depending on the culture environment. Stem cells delicately orchestrate tissue homeostasis and repair by proliferating to efficiently replace damaged tissue.[10] Stem cell-mediated tissue regeneration can also contribute to long-term tissue homeostasis and presents an ideal solution for calvarial bone regeneration. In order to mediate this process, the stem cells need to be placed in a niche environment that supports tissue regeneration. Biomaterials such as hydroxyapatite/tricalcium phosphate (HA/TCP) have been utilized as structural support for stem cell-mediated injury repair and can play an additional role in regeneration by supporting MSC function.[11-15] Advances in three-dimensional (3D)-printing technology have enabled customized design of these biocompatible materials such that they can be fit

Significance statement

The present study reveals a novel three-dimensional-printed hydroxyapatite tricalcium phosphate scaffold design and describes standardized loading dosages of dental pulp neural crest mesenchymal stem cells or bone marrow aspirate that support the regeneration of high-quality bone in a critical size defect (CSD) in swine. This discovery may have important impacts on other bone regeneration beyond the craniofacial region and will ultimately benefit patients who suffer from debilitating CSDs.

precisely to the dimensions of an injury, but few provide structural integrity that is suitable for clinical use.[16]

In this study, we have defined a clinically relevant large animal model to study calvarial CSDs and have developed an innovative, biological approach that harnesses the ability of stem cells to regenerate craniofacial bone. In comparison to previous studies using mice and rats as animal models, we have created and tested a swine model that has a head size, skull thickness, and healing rate similar to those of humans. Our innovative 3D-printed osteoconductive HA/TCP scaffold with structural integrity in combination with autologous neural crest or bone marrow MSCs promotes full healing of CSDs in the swine calvaria. Significantly, the regenerated bone forms a smooth calvarial surface with both fully functional and aesthetically satisfying results. Moreover, we show that the regenerated bone is of high quality that is comparable to their surrounding native bones. Importantly, we achieved these successful results with bone marrow aspirate (BMA), which can be easily obtained from a patient for autologous use and needs minimal manipulation, saving substantial time, resources, and avoiding possible complications from in vitro MSC expansion. This discovery represents an innovative, MSC-mediated tissue regeneration approach in a model that lays the groundwork for improving care for human patients with calvarial CSDs and has the potential to fill an unmet clinical need.

2 | MATERIALS AND METHODS

Yorkshire farm pigs at 10-12 weeks of age were used to investigate stem-cell-mediated calvarial bone regeneration. All animal procedures were performed in accordance with federal regulations and with approval from the Institutional Animal Care and Use Committee (IACUC) at the University of Southern California.

2.1 | Harvesting of swine dental pulp cells

Each pig (10-12 weeks of age) was anesthetized by veterinary staff and placed on its stomach. The inside of the mouth was wiped

sequentially with a germicide and ethanol to prevent infection. The right mandibular incisor was extracted and the remaining gap was closed with discontinuous, absorbable vicryl monofilament sutures in size 3-0. Dental pulp neural crest mesenchymal stem cells (DPNCCs) were harvested from the incisor and expanded in cell culture as described below.

2.2 | Culture of swine dental pulp cells

After extraction of the incisor, the outside of the tooth was thoroughly scrubbed with gauze soaked in bleach for 2 minutes to eliminate oral microbes. The tooth was cut open using sterile dissection scissors or a diamond burr. The dental pulp was removed using blunt, sterile forceps. The dental pulp was then finely chopped using sterile scissors and digested with a 0.2% solution of Collagenase Type I (Washington Biochemical Corporation, Table 1) diluted with Alpha-MEM (Gibco, Table 1) in a water bath at 37°C for 1.5 hours. The dental pulp-containing Collagenase solution was then strained for single cells using a 70 μm cell strainer into a 50 mL conical tube. The remaining solution was centrifuged at 1440 rpm for 5 minutes at 21°C and the supernatant was discarded. The cell pellet was resuspended in culture media and plated at 1×10^6 cells per 15 cm tissue culture dish. Cells were incubated at 37°C and 5% CO_2.

Cells were cultured at low density to form single-cell colonies, and were passaged once reaching 65-70% subconfluence. To passage, media was removed from the culture dishes and the cells were washed with DPBS (Gibco, Table 1). After removal of DPBS, cells were detached from the plates using TryplE Express with Phenol Red (Gibco, Table 1) for 7 minutes at 37°C and 5% CO_2. The cells and enzyme solution were immediately transferred to a conical tube with an equal volume of culture media to deactivate the enzyme. This solution was used for cell counting as described below, then centrifuged. The supernatant was discarded and the cell pellet was resuspended in culture media. With each passage, 1×10^6 cells were plated into 15 cm dishes. This process was repeated 2-3 times over 14 days before transplantation into the calvarial defect. Cells were counted using a BioRad TC20 Automated Cell Counter. Ten microliters of suspended cells were loaded into the cartridge for cell counting. For transplantation, three 10 μL suspensions were counted and averaged. For each animal, $3-4 \times 10^6$ autologous cells were transplanted into

the CSD site (see below) with HA/TCP particles or an HA/TCP 3D-printed scaffold.

Cells for the heat-inactivated DPNCC group were prepared and passaged using the same method as living DPNCCs. At the time of the last passage for transplantation, the cells were again detached from plastic plates using TriplE for 7 minutes at 37°C and 5% CO_2 and transferred to a conical tube. An equal volume of media was added to this solution before the cells were counted using a BioRad TC20 Automated Cell Counter as described above. Cells were centrifuged at 1440 rpm for 5 minutes, the supernatant was discarded, and the remaining cell pellet was resuspended in 1 mL of culture media. The resuspension was transferred to a sterile centrifuge tube and heated to 85°C for 20 minutes. There were no live cells following the heat treatment.

With the remaining living cells not used for transplantation to support calvarial bone regeneration, the ability of the DPNCCs to differentiate into adipocytes, chondrocytes, and osteoblasts was verified through culture in adipogenic, chondrogenic, and osteogenic culture media, respectively (Gibco, Table 1). Adipogenic differentiation was evaluated using Oil Red O staining for lipid droplets. Chondrogenic differentiation was evaluated using Alcian blue staining for cartilage formation following condensation of cultured DPNCCs.[17] Osteogenic differentiation was evaluated using Alizarin red staining for bone formation.

2.3 | Application of DPNCCs and HA/TCP nanoparticles or 3D-printed HA/TCP scaffold to swine calvarial CSD

Cells were washed with DPBS and dissociated from the culture dish as described for passaging above. For each calvarial CSD (3.0 cm in diameter), $3-4 \times 10^6$ autologous cells were transplanted into the defect site. For experimental groups using HA/TCP nanoparticles, the cells were resuspended in 3 mL culture media. Cells were placed on ice and transported to the operating room in a styrofoam container. During surgery, the 3 mL suspension was mixed with 5 g HA/TCP sterile nanoparticles (Sigma-Aldrich) in a sterile bowl until a paste-like consistency was reached. The DPNCC-HA/TCP paste was then transplanted into the CSD using a micro-spoon or chisel. The paste was manipulated to uniformly fill the defect and, at the surface, to follow the contours of the surrounding parietal bone.

TABLE 1 Cell culture reagents

Reagent name	Company	CAT/REF#	LOT#
Collagenase type I	Washington Biochemical Corporation	CAT#: LS004194	LOT#: 45D15720
DPBS, no calcium, no magnesium	Gibco	CAT#: 14190250	
Alpha-MEM	Gibco	REF#: 12571-063	LOT#: 2044318
TryplE Express with Phenol Red	Gibco	REF#: 12605-010	LOT#: 1897328
Adipogenic differentiation media	Gibco	REF#: A10410-01	LOT#: 1925522
Chondrogenic differentiation media	Gibco	REF#: A10069-01	LOT#: 1929138
Osteogenic differentiation media	Gibco	REF#: A10069-01	LOT#: 1929138

For groups using an HA/TCP 3D-printed scaffold, cells were resuspended in 0.5-1 mL culture media. Cells were placed on ice and transported to the operating room in a styrofoam container. During surgery, the 3D-printed HA/TCP scaffold was first sized and placed into the defect (3.0 cm in diameter circular defect). Any excess scaffold was shaved off using a scalpel or forceps. After placement of the scaffold, the cell suspension was evenly loaded onto the entire scaffold using a 1 mL syringe without a needle.

2.4 | BMA collection in swine

In order to compare the ability of BMA to DPNCCs in supporting calvarial bone regeneration, we harvested bone marrow from the swine tibia. After anesthesia by veterinary staff, the animal was placed in lateral recumbency. The tibia was shaved and cleaned three times

sequentially with germicidal scrub and 70% ethanol. A bone punch was used on the medial aspect of the proximal tibia, where the bone is not covered by muscle[18] (Figure 2G,H). This was confirmed by palpating the area. Once the needle penetrated the bone cortex, 4-8 mL bone marrow was collected using a syringe. For the 3 cm defect, 4 mL bone marrow was centrifuged at 2400 rpm for 9 minutes using the Harvest SmartPrep System. The serum supernatant was discarded and the remaining cells were loaded into the 3D-printed HA/TCP scaffold using a 6 mL syringe without a needle.

2.5 | Culture and differentiation of swine bone marrow MSCs

Swine bone marrow was collected from tibial crest into tubes containing an anticoagulant. The bone marrow was divided into 10 mL
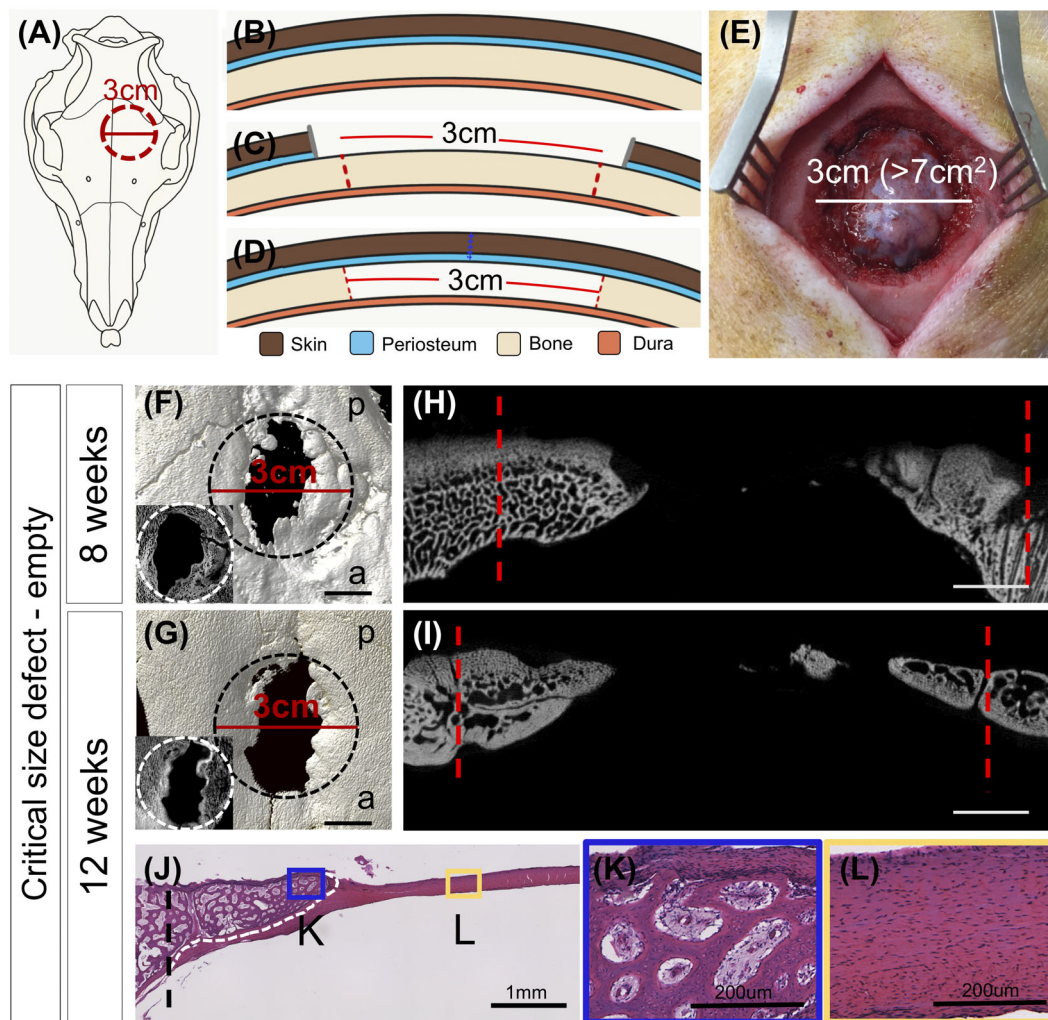
FIGURE 1 Generating a critical-sized defect in the swine calvaria. Schematic drawing of defect placement (A) on the swine calvarial surface. Schematic drawing in coronal view of (B) normal calvarial bone, periosteum, skin, and dura; C, retraction of the skin and periosteum to expose bone to create 3 cm defect; D, skin and periosteum closure over bone. E, Gross anatomy image of empty defect at time of surgery showing exposed dura. MicroCT showing defect at (F, H) 8 weeks post-surgery and (G, I) 12 weeks post-surgery. F and G, Inserts show transverse microCT through defect. Red dashed lines (H, I) indicate boundary of defect site. J-L, Histological sections of defect at 12 weeks post-surgery. Boxed areas in J are shown enlarged in K and L. Scale bar = F-G, 10 mm; H-I, 5 mm; J, 1 mm; K-L, 200 μm

aliquots, further diluted with PBS to 30 mL and mixed well. Then 10 mL Ficoll-Paque Plus was slowly added to the bottom of the tube, followed by centrifugation at 20°C for 30 minutes at 400g with slow acceleration. The middle layer was collected into a new tube containing 25 mL PBS. This new tube was centrifuged at room temperature for 7 minutes at 350 g and the supernatant was removed. The cell pellet was resuspended with MSC culture medium and the cells were plated in a 10 cm culture dish. The medium was changed once every 3 days, and colonies of MSCs were visible after 7-10 days.[19]

2.6 | Creating the CSD in swine

Each pig was anesthetized by the veterinary staff and placed on its stomach. The cranial surface was shaved and then cleaned sequentially with Betadine and 70% ethanol. A scalpel was used to make a 7-8 cm incision in the skin, about 1 cm left of the midline. A periosteal elevator was used to lift the periosteum from the calvarial bone. Once the underlying bone was exposed and surrounding skin and periosteum were retracted, the CSD of 3 cm in diameter was measured and marked on the bone. An oscillating saw was used to cut into the bone. When approaching the deep portion of the bone, a hammer and chisel were used to create the full-thickness defect so as not to damage the dura or brain below. Once the bone was removed, HA/TCP

nanoparticles were mixed with cells and loaded into the defect site. For experimental groups using the 3D-printed HA/TCP scaffold, the HA/TCP scaffold was sized and loaded into the CSD first, then cells were injected into the holes of the scaffold using a syringe. Control CSDs were left empty after removal of the bone. The incision was then closed in layers, with the periosteum and loose connective tissue closed first and the superficial skin sutured second. Simple interrupted ties were made using 3-0 vicryl absorbable sutures (deep layer) and 0 nylon non-absorbable sutures (superficial layer). The defect was allowed to heal over 8 or 12 weeks or 6 months.

2.7 | Dissection and collection of swine calvaria

Eight or twelve weeks or six months after implantation, each animal was first anesthetized then euthanized by overdose of pentobarbital. The animal was then decapitated. A scalpel was used to make an incision in the skin along the midline of the calvaria, and a periosteal elevator was used to expose the underlying bone over the defect area. All soft tissue was separated from the surface of the bone using a scalpel and periosteal elevator. The sample was fixed in 10% formalin overnight, then placed in 1x PBS solution for CT imaging of the entire skull and calvarial surface. Once the whole skull was imaged, the calvaria surrounding the defect (about 6 × 6 cm) was dissected using a
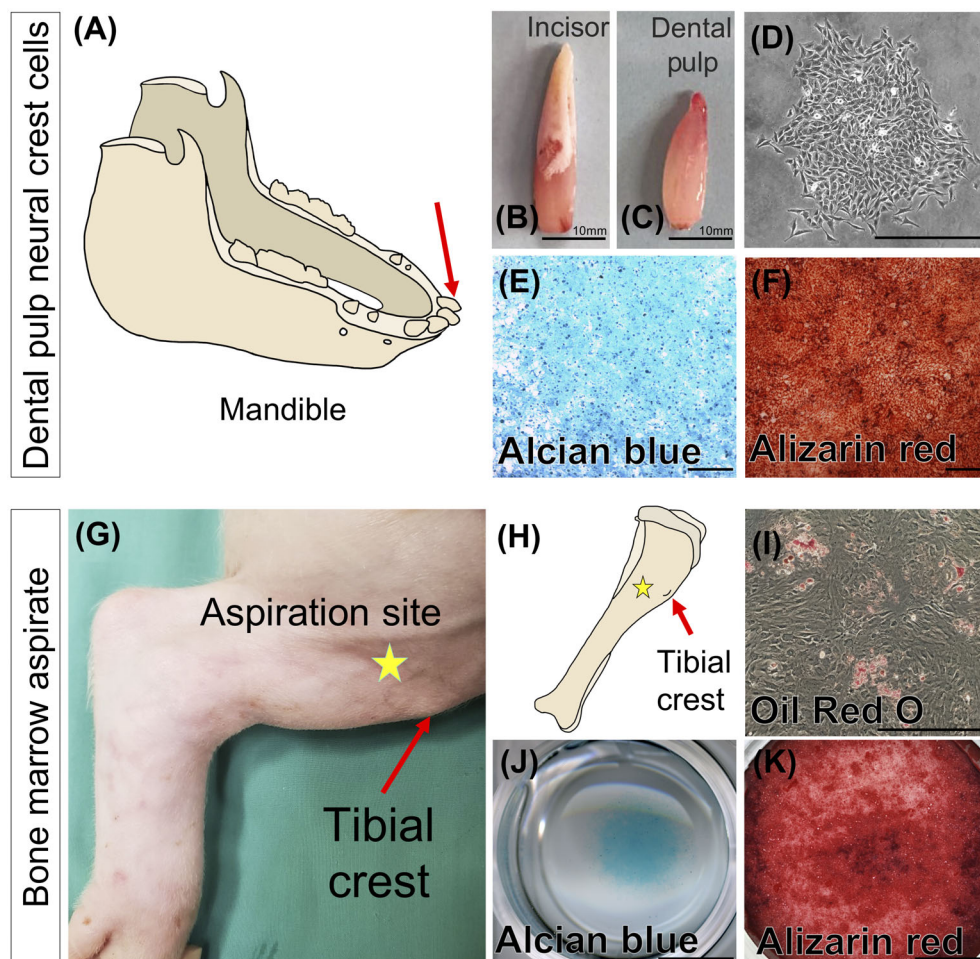
FIGURE 2 Harvesting and characterization of dental pulp-derived neural crest cells. A, Schematic drawing of swine mandible. Red arrow indicates location of extracted swine incisor. B, Swine incisor post-extraction and, C, dental pulp removed from incisor. D, Single-cell colony of undifferentiated DPNCCs, 48 hours after extraction and plating. E, Alcian blue staining of DPNCCs, 3 weeks post-plating. F, Alizarin red staining of DPNCCs, 1 week post-plating. G, Photo of swine tibia at time of bone marrow aspiration, indicating the tibial crest landmark and site of aspiration. H, Schematic drawing of tibial bone with aspiration site. I, Oil Red O staining of BMA, 1 week post-plating. J, Alcian blue staining of BMA culture, 3 weeks post-plating. K, Alizarin red staining of BMA culture, 1 week post-plating. Scale bar = B-C, 10 mm; D-F, I, 200 μm; J-K, 5 mm

cordless reciprocating DeWalt saw with wood-cutting blades. The sample was again fixed in 10% formalin overnight, then placed in DPBS for further microCT imaging.

2.8 | Development of the 3D-printed osteoconductive scaffold

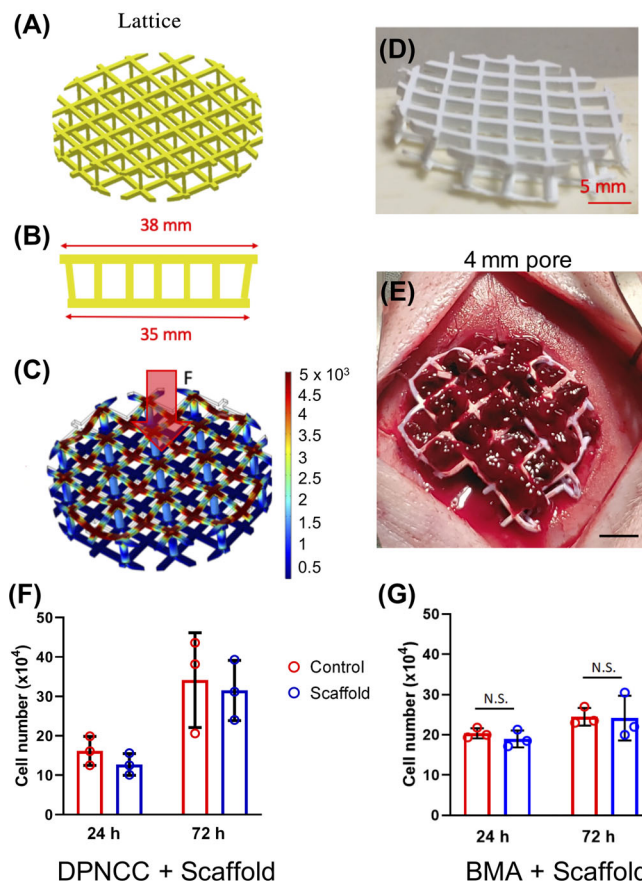### 2.8.1 | HA/TCP scaffold design

The scaffold was designed based on the dimensions of a swine CSD extracted from CT scanning (Figure 1E). Specifically, a 3D digital model of the injured swine calvarial bone was generated using Avizo software, and a digital model of the craniofacial defect was generated based on the contours of the CSD. This determined the overall shape and dimensions of the scaffold. Next, computer-aided design software was used to design micro-cell structures in the central portion of the scaffold.[20] A set of digital design tools were developed and used for scaffold construction, enabling design of a scaffold with desired porosity and mechanical strength.[21,22] Lattice structure scaffolds of pore size 4 mm were transplanted into the swine calvaria in combination with dental pulp- or bone marrow-derived MSCs. The compressive strength of each scaffold was simulated using Comsol MultiPhysics (Figure 3C).

2.8.2 | HA/TCP printing material preparation

Hydroxyapatite (HA) powder with a particle size of 10 µm was purchased from Sigma-Aldrich (CAS#: 1306-06-5). Tricalcium phosphate (TCP) with a particle size of 4 µm was also purchased from Sigma-Aldrich (CAS#: 12167-74-7). The photo-curable liquid polymer WaxCast (purchased from MakerJuice LABS) was used as a polymer binder. First, HA/TCP slurry (30 wt%) was prepared. HA (15 wt%) and TCP (15 wt%) were poured into the liquid photopolymer resin (WaxCast) sequentially, and the HA/TCP mixture was ball-milled with a rotational speed of 200 rpm for 40 minutes. After that, the HA/TCP powders were homogenously distributed inside the photocurable resin and the HA/TCP slurry was degassed under a vacuum prior to the printing process.

2.9 | 3D printing and post-processing of HA/TCP scaffold

A mask image projection-based slurry printing (MIP-SP) process was developed to enable fabrication of HA/TCP microparticles, as described by Li et al.[20] The digital model of the 3D craniofacial scaffold was first imported into the software we developed, and a set of 2D mask images was obtained by slicing the digital model with 75 µm layer thickness. This layer thickness was determined by the cure depth of the HA/TCP slurry. During the printing process, the photocurable polymer mixed with HA/TCP particles selectively underwent

FIGURE 3 Design and fabrication of HA/TCP scaffold using 3D printing and light-curing. A, Digital model of the custom designed scaffold showing dimensions; B, digital model of the lattice design 3D-printed HA/TCP scaffold and measurements from the side view; C, simulation of HA/TCP scaffold under compression using Comsol MultiPhysics; D, image of final scaffold product; E, Gross anatomy photo of scaffold loaded with cells in the 3 cm defect at time of surgery. Cell compatibility studies for (F) DPNCC and (G) BMA culture with HA/TCP scaffold. Scale bar = 5 mm

photopolymerization, which was activated by the radiation of ultraviolet light with a specially designed pattern. The cured HA/TCP slurry was deposited layer by layer (100 µm thickness, to allow for shrinkage) to form the 3D shape. To remove the polymer and improve mechanical performance, the scaffold was debinded in a tube furnace (MTI Corp) at a temperature higher than 650°C for 180 minutes. After this debinding process, the scaffold was allowed to cool to room temperature naturally. Next, to fuse the ceramic particles together, the scaffold underwent a sintering process. A tube furnace (MTI Corp) was used to heat the scaffold to 1150°C for another 3 hours. The finalized HA/TCP scaffold was then cooled to room temperature. Scaffolds were individually autoclaved before surgical use.

2.10 | Cell viability analysis

DPNCCs and BMA were independently seeded at 2.5×10^4 per well in a 48-well plate and allowed to rest for 24 hours for attachment.

Then, 3D-printed HA/TCP scaffolds were co-cultured with the cells to test their effect on cell proliferation. Cells were harvested at 24 and 72 hours and quantified using the BioRad Cell Counter as described above.

2.11 | MicroCT imaging, density, and trabecular bone analysis of calvarial samples

MicroCT analysis was performed using a SCANCO µCT50 (Scanco V1.28) at the University of Southern California Molecular Imaging Center. The microCT images were acquired from swine 8 or 12 weeks or 6 months after calvarial injury with the X-ray source at 70 kVp and 250 µA. The data were collected at a resolution of 12.3 µm. Reconstruction in 3D was achieved using Avizo 7.1 (Visualization Sciences Group). The background noise from these segmentations and bones outside the scope of this study, such as the neck vertebrae, were manually removed using Avizo's editor tools (Threshold, Contrast, Cropping).

2.12 | Compression testing of regenerated bone and native bone

Compression testing was performed using INSTRON 5944 Universal Testing Systems up to 2 kN (450 lbf) force capacity. A 50 mm compression plate was used as the stationary stage. The compressive arm was made of a 1 cm diameter probe held by a 3-jaw chuck (INSTRON CAT#: 2830-036). To test compressive and mechanical strength, each sample was placed on the stage such that when the compressive arm lowered, a specific location on the bone was compressed. We tested three locations within the defect area (with or without bone regeneration) and three locations on the surrounding native bone for each sample. The compressive arm moved at a rate of 0.2 cm/s. For each location, the force applied by the arm and the displacement of the arm were measured. The end-of-test criteria were: (a) the force that needed to be applied exceeded the capacity of the system, (b) a 40% drop in force was observed, or (c) the moving arm met the stationary stage.

2.13 | Decalcification and histological analysis of swine calvaria

After imaging, samples were decalcified using 20× sample volume of Leica Decalcifier I reagent. Samples were placed on a shaker and monitored every week for 3 months. The solution was changed every 2 weeks. Once pliable enough, the sample was cut down into smaller pieces to reduce the decalcification and dehydration time. Decalcification progress was examined using microCT analysis to verify presence or absence of calcified bone. Once fully decalcified, samples were dehydrated using increasingly concentrated solutions of ethanol (30%, 50%, 70%, 80%, 90%, 100%) then Xylene, a solution of 50:50 Xylene:

paraffin, and paraffin. The samples remained in each solution for 12 hours then fixed in paraffin. SupaMega Stainless Steel Base Molds (Electron Microscopy Sciences, Supplier #:62354-60) were used to embed these samples. Paraffin-embedded samples were sectioned on a microtome with slices of 10-25 µm thickness. Sections were plated on SupaMega slides and stained with hematoxylin and eosin (H&E) as previously described.[23] Slides were imaged using a Keyence BZ-X710 fluorescence microscope in brightfield setting.

3 | RESULTS

3.1 | Creating a critical size defect model in the swine calvaria

In swine, the definition of a critical-sized defect (CSD) in the calvaria has not yet been fully established in the literature. More generally, a CSD is an injury that will not heal completely over the lifetime of the animal, or more conservatively, over the time course of the study in question, if no intervention is made.[24] It has been reported that a defect with 10 mm width and 10 mm thickness in swine craniofacial bone meets this criterion.[25] We decided accordingly to create a round, full-thickness defect with a diameter of 3 cm (area >7 cm^2) in the Yorkshire farm pig calvaria (Figure 1A-E). MicroCT imaging showed minimal bone regeneration at the edges of the defect and no bone tissue at the center of defect at either 8 or 12 weeks post-injury (Figure 1F,G). Histological analysis confirmed that only soft tissue was found in the defect at 12 weeks post-surgery (Figure 1J-L). Spanning each defect there was a layer of soft tissue approximately 0.5 mm thick (Figure 1J), leaving minimal protection for the brain in this area. The 3 cm diameter defects in control swine without cells or HA/TCP failed to heal over the course of 8 weeks (Figure 1F,H), and we confirmed that a defect of this size would also fail to heal within 12 weeks (Figure 1G,I). Therefore, we have established a swine calvarial CSD model as a defect of 3 cm in diameter, which will not normally heal within 12 weeks following surgical removal of the calvarial bone.

3.2 | Comparison of dental pulp neural crest MSCs and BMA

In the last decade, mesenchymal stem cells (MSCs) have been widely used for regenerative therapies due to their ability to maintain stemness and to differentiate into many cell types, including but not limited to osteocytes, chondrocytes, and adipocytes. Previous studies have shown that in combination with HA/TCP, cranial neural crest-derived MSCs regenerate mainly dense cortical bone while bone marrow-derived MSCs regenerate trabecular bone with marrow space.[17] We hypothesized that cranial neural crest-derived MSCs would regenerate the dense craniofacial bone necessary for our calvarial injury model but that BMA may also be adequate to support calvarial bone regeneration. Clinically, autologous dental-derived MSCs

can be obtained from dental pulp, which is limited in supply, and must be expanded in vitro before transplantation. BMA is more commonly used for bone regeneration clinically, does not need to be expanded in culture, and is relatively more abundant while still being relatively simple to collect from the patient. In our study, we tested the regenerative potential of dental pulp neural crest MSCs (DPNCCs) from the dental pulp and compared it to that of BMA when each of these cell sources were used in combination with our 3D-printed HA/TCP scaffold in the swine calvarial CSD model. Our comparison is intended to inform future clinical practice of stem cells mediated bone regeneration in CSDs.

DPNCCs collected from the swine lower incisor (Figure 2A-C) were cultured at low density in order to promote single cell colony formation. Within 24-48 hours of plating, cells attached to the bottom of the plastic dish. Cells maintained a rounded shape until fully attached to the plate. Once attached, cells began to elongate and spread (Figure 2D), and their morphology remained consistent for the remainder of the culture period. Every 4-5 days, cells reached approximately 70% confluence and were passaged. After 2 weeks, DPNCCs were transplanted into the calvarial defect to support bone regeneration.

In a comparison group, bone marrow was aspirated from the swine tibia while the animal was anesthetized for the creation of the calvarial CSD (Figure 2G,H). The aspirate was centrifuged and remaining cells were transplanted into the calvarial defect.

To test the stem cell properties of the DPNCCs and BMA, both were separately cultured and differentiated toward different cell fates. DPNCCs and cells derived from BMA were successfully differentiated into chondrocytes, as confirmed with Alcian blue staining (Figure 2E,J), and also successfully differentiated into osteocytes, as confirmed with Alizarin red staining (Figure 2F,K). In addition, BMA-derived cells were able to differentiate into adipocytes (Figure 2I). Collectively, these experiments demonstrate the stemness of these DPNCCs and BMA cells.

3.3 | DPNCCs with HA/TCP nanoparticles regenerate bone in full-thickness calvarial CSDs

To test the regenerative potential of DPNCCs with HA/TCP, we treated 3 cm diameter calvarial CSDs in swine with 4×10^6 DPNCCs +5 g HA/TCP nanoparticles and compared them to controls (unfilled CSDs) after 8 weeks. We observed a significant difference in bone regeneration between control swine (n = 3) and those which received HA/TCP and DPNCCs (n = 3). Calvarial bone CSDs treated with HA/TCP particles and DPNCCs showed complete calvarial bone regeneration and normal bone density when compared with the native calvarial bone (n = 3, with 100% success rate) (Figure S1A,B). In the control group, however, there was no bone formation within the CSD (Figure 1F,H) in the swine after 8 weeks.

To test the functional significance of DPNCCs in supporting calvarial bone regeneration in swine, we tested the ability of fibroblasts or heat-inactivated DPNCCs combined with HA/TCP particles to support calvarial bone regeneration. Autologous gingival fibroblasts ($3\text{-}4 \times 10^6$) combined with HA/TCP particles were placed in the calvarial defect site (n = 3) following the same procedure. Eight weeks later, we did not observe any calvarial bone regeneration within the CSD with CT analysis (Figure S1F,G). As with the defects with neither cells nor HA/TCP, we observed a layer of soft tissue filling the CSD site but there was no bone formation. Similarly, heat-inactivated DPNCCs transplanted with HA/TCP nanoparticles failed to support bone regeneration to heal the CSDs, as there was no new calvarial bone regeneration observed via microCT 8 weeks after surgery (n = 3) (Figure S1K,L).

Taken together, this series of experiments demonstrated that living MSCs combined with HA/TCP can successfully support calvarial bone regeneration, whereas fibroblasts or heat-inactivated MSCs delivered with HA/TCP cannot, nor can HA/TCP alone. Despite the successful regeneration of calvarial bone in a CSD using DPNCCs and HA/TCP, the possibility remained that the regenerated calvarial bone could be aesthetically improved with a smoother surface (Figure S1A). We hypothesized that our osteoconductive 3D-printed scaffold would assist in the uniform distribution of stem cells in the defect, supporting the proper formation of calvarial bone structure and producing a natural bony surface.

3.4 | Optimization of the 3D-printed osteoconductive scaffold

To improve the surface anatomy of regenerated calvarial bone, we designed and fabricated a 3D-printed biodegradable scaffold based on a CT scan of a calvarial CSD in an adult farm pig. The scaffold was designed with a lattice structure to support transplanted MSCs (Figure 3A-D). This lattice design allowed for easy cell loading, while providing adequate protection of the brain tissue under the CSD. The details of the 3D-printing process developed to fabricate the HA/TCP scaffold have been described previously.[20,21] The top surface of the designed scaffold was a circle of 3.8 cm diameter and it tapered down to a bottom surface with 3.5 cm diameter (Figure 3B). The bottom was concave and closely matched the curvature of the inner skull surface. In addition, the 3D-printed scaffold was designed to be filled with cells via 4 mm holes. The final scaffold had a disc-like shape of the desired dimensions so that it fit precisely into the swine calvarial CSD (Figure 3E). The compressive strength of the scaffold, as simulated using Comsol Multi-Physics Mechanical software, enabled it to maintain its shape during handling and after surgery (Figure 3C).

To test how DPNCCs or BMA combined with 3D-printed HA/TCP scaffold may support calvarial bone regeneration in a CSD, we created a calvarial CSD 3 cm in diameter as described above. The 3D-printed HA/TCP scaffold was gently placed into the defect and loaded with DPNCCs or BMA via a syringe. The surgical site was then sutured closed. A cell viability study showed that each cell type was compatible with the scaffold in vitro and thus suggested it would be safe for use in vivo (Figure 3F,G).

3.5 | MSCs combined with 3D-printed osteoconductive scaffold improve the quality of regenerated calvarial bone

To test the potential of MSCs delivered with 3D-printed HA/TCP scaffold for stem cell-mediated bone regeneration in the swine calvaria, we generated a CSD (3 cm in diameter) in the swine calvaria as outlined above. Following transplantation of the 3D-printed HA/TCP scaffold with DPNCCs (3-4 × 10^6 autologous DPNCCs) into the calvarial CSD, we monitored the bone regeneration at 8 (n = 6) and 12 (n = 3) weeks. At 8 weeks, the injury had healed throughout the entire CSD (Figure 4E,F). The bone was thickest at the edges of the defect, suggesting that it began to regenerate from the edges and progressed inward. The regenerated bone appeared continuous with the native bone based on surface appearance and CT analyses (Figure 4E,F). Histological staining showed stripes of cortical bone between areas of trabeculation, with more trabecular structures at the edge of the defect and thick, dense stripes of new bone at the center of the defect (Figure 4G,H). Newly regenerated bone surrounded the scaffold material and formed a bone network around the remaining HA/TCP material (Figure 4G). At 8 weeks post-surgery, density analysis showed that the regenerated bone was significantly less dense than the surrounding native bone (P = .0137, Figure 6A). To assess the quality of the newly regenerated calvarial bone, we conducted compression tests. The maximum force that was able to be applied to bone regenerated using DPNCCs and HA/TCP matched that of the surrounding native bone. Furthermore, the displacement of the compressive arm at maximum force was the same between native and regenerated bone. In the control group, the CSD area showed no resistance to the compression force, indicating that DPNCCs and our HA/TCP scaffold successfully supported calvarial bone regeneration in comparison to the control group 8 weeks post-surgery (Figure S2A). No defects in the dura or brain were observed under the CSD area when treated with DPNCCs and scaffold, suggesting that the scaffold protected the vital structures (n = 9). No adverse effects to the animals were observed from the surgical procedure or treatment with the DPNCCs and scaffold (n = 9). There was no ectopic bone nor abnormal tumor-like tissue formation in any of the calvarial CSDs treated with DPNCCs and 3D-printed HA/TCP scaffold after 8 or 12 weeks.

At 12 weeks post-injury (n = 3), the surface of the newly regenerated bone appeared to be smoother than at 8 weeks post-injury (Figure 4I). The regenerated bone formed a continuous connection with the native bone and showed uniform bone formation throughout the CSD (Figure 4I,J). The HA/TCP scaffold underwent further degradation, but some HA/TCP remained. The regenerated bone formed a complex network resembling the endogenous bone structure (Figure 4K,L). Histological H&E staining showed new, dense, cortical bone surrounding the remaining HA/TCP scaffold (Figure 4K). The mean trabecular number of the regenerated bone was not significantly different from that of the native bone at 12 weeks post-surgery (Figure 6D). The trabecular spacing and thickness of the newly formed bone indicated that the regenerated bone in the CSD had begun
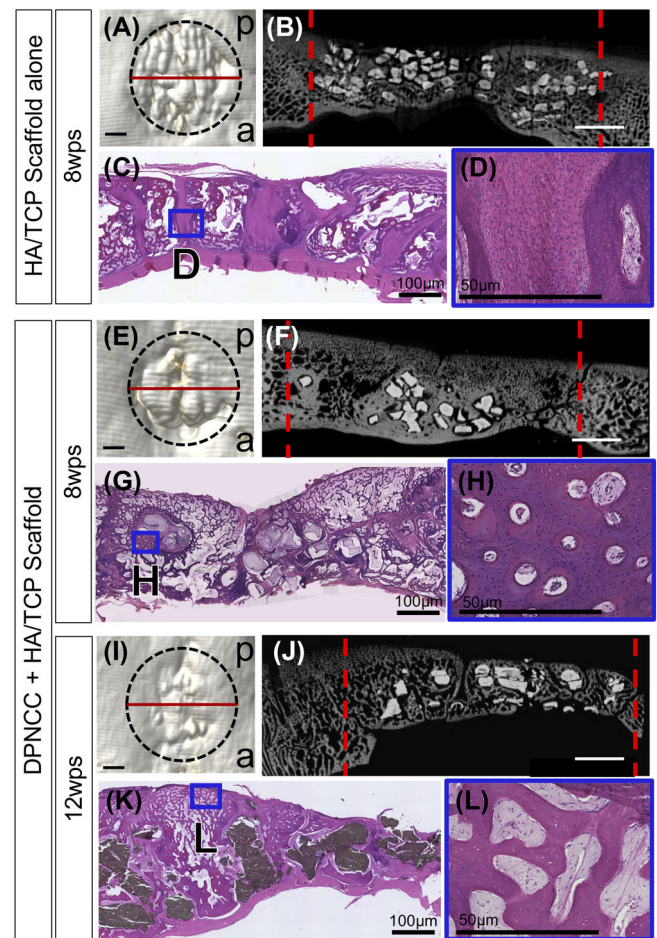

FIGURE 4 Dental pulp-derived MSCs and 3D-printed scaffold regenerate dense, strong bone in the swine calvarial CSD. MicroCT of CSD filled with (A, B) HA/TCP scaffold alone; E and F, HA/TCP scaffold with DPNCCs imaged 8 weeks post-surgery; I and J, HA/TCP scaffold with DPNCCs 12 weeks post-surgery. C-E, H-J, and M-O, Histological staining of defect filled with HA/TCP scaffold (C, D) alone or in combination with DPNCCs at (G, H) 8 weeks post-surgery and (K, L) 12 weeks post-surgery. Black and red dashed lines indicate original site of injury. Scale bar = A-B, F-G, K-L, 10 mm; C-E, H-J, M-O, 1 mm

remodeling as the ones in the native calvarial bone. The density of the regenerated bone at 12 weeks post-surgery was comparable to the native bone, as indicated by CT analysis (Figure 6B). Compression testing of the regenerated bone from DPNCC + 3D-printed HA/TCP scaffold samples showed comparable strength to the native bone (Figure S2B). During compression testing, cracking of the samples never occurred at the junction between the newly formed and native bone.

3.6 | BMA and 3D-printed scaffold in calvarial bone regeneration to repair CSDs

To test the potential of BMA to regenerate calvarial bone in swine, we collected 4 mL of bone marrow from the swine tibial crest. After

FIGURE 5 Bone marrow aspirate and 3D-printed scaffold regenerate dense, strong bone in a swine calvarial CSD. MicroCT of critical size defect filled with HA/TCP scaffold of 4 mm pores with bone marrow aspirate (A, B) imaged 8 weeks post-surgery and (E, F) 12 weeks post-surgery. C, D, G, and H, H&E staining of defect filled with BMA + HA/TCP scaffold (C, D) 8 weeks and (G, H) 12 weeks post-surgery. Black and red dashed lines indicate original site of injury. Scale bar = A-B, E-F, 5 mm; C, G, 1 mm; D, H, 0.5 mm
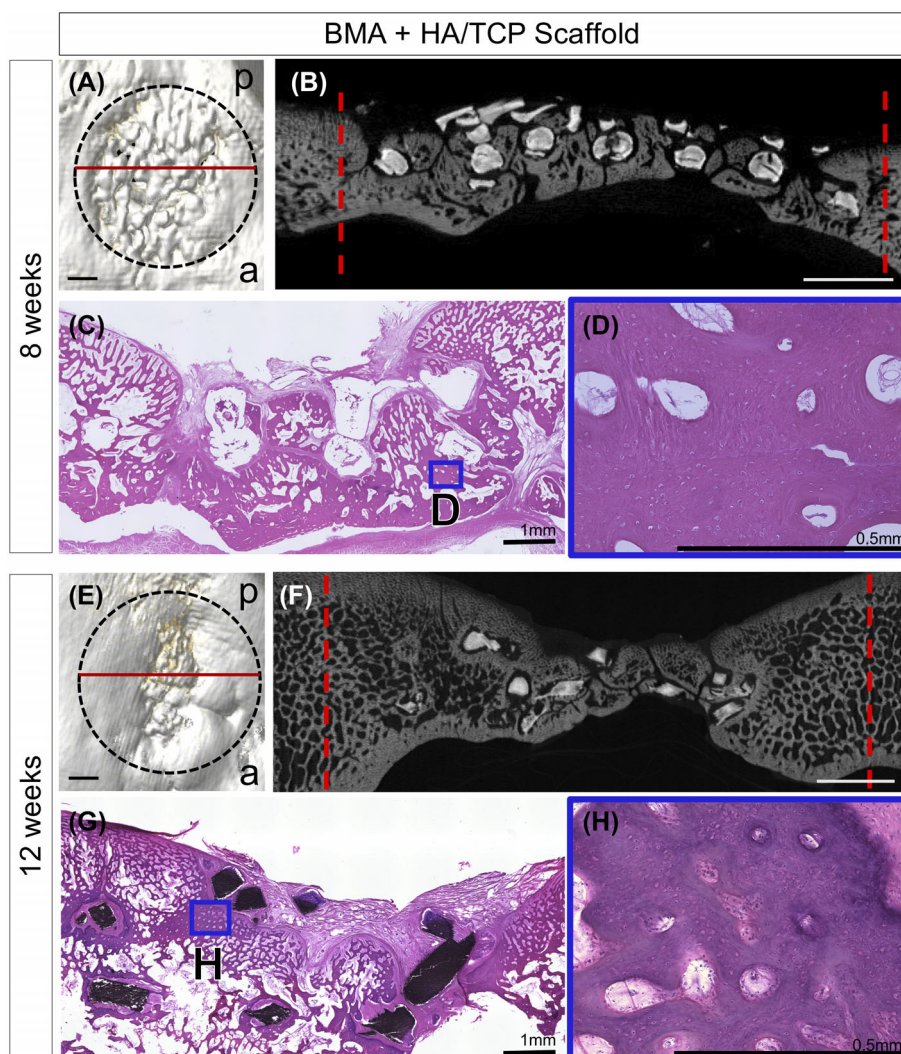

centrifuging, the remaining BMA containing MSCs was transplanted into a 3D-printed scaffold and subsequently placed into a 3 cm diameter defect in the calvarial bone CSD (n = 8).

As with DPNCCs, the BMA was able to regenerate bone in this CSD in the presence of the 3D-printed HA/TCP scaffold. At 8 weeks, the bone defect was healed throughout, and similar to the DPNCC-treated group (n = 4). CT imaging analyses suggested that the new bone growth began at the edges of the defect and progressed toward the center (Figure 5A,B). During the study, no animals experienced any complications or infections related to the calvarial surgery, bone marrow retrieval site, or treatment with BMA and HA/TCP scaffold. Upon dissection, the defect site was smooth to the touch. Upon visual inspection, the newly formed bone resembled the surrounding calvarial bone in color and texture. Density of the regenerated bone was not significantly different from that of the native bone (Figure 6A). MicroCT analysis showed that a trabecular network formed around the remaining scaffold and integrated with the surrounding native bone (Figure 5B). Trabecular structure analysis showed that the regenerated bone had similar trabecular thickness with increased trabecular number and decreased trabecular spacing as compared with the native calvarial bone at 8 weeks post-surgery (Figure 6C).

Histological analysis of these samples confirmed the complex trabecular network shown in the microCT images (Figure 5C,D). The regenerated bone was dense and cortical, as indicated in our H&E staining at 8 weeks post-surgery (Figure 5C,D). Some HA/TCP material persisted within the regenerated calvarial bone. During compression testing, the regenerated bone performed similarly to the native bone (Figure S2A). None of the samples broke at the junction between native and regenerated calvarial bone.

During dissection of the calvaria samples of 12 weeks post-surgery, we observed less remaining HA/TCP scaffold material as compared with the samples at 8 weeks post-surgery (n = 4) (Figure 5F). The boundary of the original defect was undetectable both upon visual inspection and in microCT images (Figure 5E,F). The bone density and compressive strength of the newly regenerated calvarial bone were comparable to those of the native bone (Figure 6B). Furthermore, these samples never broke at the junction of new and regenerated bone during compressive testing. At the center of the original CSD, the regenerated bone appeared to be thinner than at the periphery of the defect, suggesting that new calvarial bone formation initiated from the edge of the CSD (Figure 5E,F). Our histological analysis indicated that there was dense calvarial bone regeneration
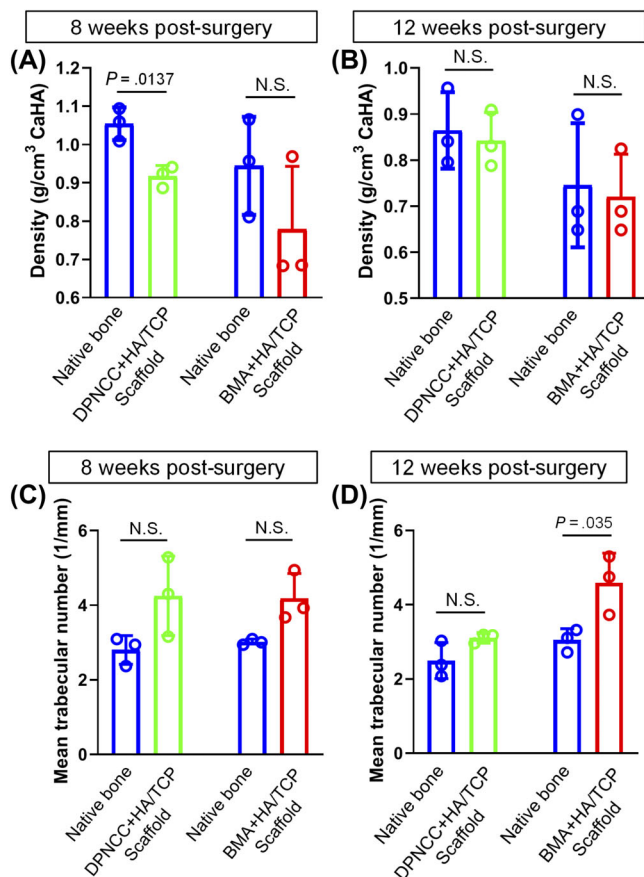
FIGURE 6 Density and trabecular analysis of calvarial bone regenerated by DPNCCs and BMA in combination with a 3D-printed HA/TCP scaffold. Density analysis comparing native bone to DPNCC- and BMA-mediated regenerated bone at (A) 8 weeks and (B) 12 weeks post-surgery. Comparison of trabecular number in native bone to DPNCC- and BMA-mediated regenerated bone at (C) 8 weeks and (D) 12 weeks post-surgery. Scale bar = 5 mm

throughout the CSD (Figure 5G,H). The remaining HA/TCP scaffold was surrounded by newly formed cortical bone (Figure 5G).

Eight and twelve weeks post-surgery, CT imaging revealed that remnants of the scaffold persisted in the healed defect in both DPNCC and BMA groups (Figure 4F,J; Figure 5B,F). Interestingly, in the scaffold-only groups, nearly the entire scaffold remained, leaving the surface uneven (Figure 4A,B). This indicates that the transplanted cells play an important role in scaffold biodegradation and may integrate the components of HA/TCP to regenerate bone in the CSD defect in the calvaria. Histological analysis of the scaffold-only groups showed growth of large strips of soft tissue accompanied by small strips of bone, suggesting the necessity of adding cells to facilitate proper bone regeneration (Figure 4C,D).

4 | DISCUSSION

This study represents a novel approach to addressing a long-standing clinical need, namely a biological solution to repair critical-sized bone defects in the calvaria. Current therapies for large calvarial bone

defects include metal and plastic implants, as well as autologous bone grafts when sufficient bone is available. There are many limitations to these therapies, particularly in the case of non-resorbable plates, which provide a purely mechanical solution to protect the brain and improve aesthetics. Metal and plastic implants are prone to infection, are uncomfortable for the patient, and do not accommodate for brain and skull growth in pediatric patients. Since these implants are not biological, they cannot integrate fully with the native bone, nor can they contribute to tissue homeostasis. Autologous bone grafts cause further harm to the patient at the harvest site and often do not yield enough bone to heal a defect of critical size. Our strategy for regenerating calvarial bone provides several distinct advantages over current clinical practice, owing to the ability of the newly regenerated bone to integrate with existing bone and participate in maintaining tissue homeostasis. Importantly for pediatric indications, calvarial bone regenerated using our approach will be able to grow with the skull and accommodate crucial future brain growth.

Skull injury repair has primarily been investigated in small animal models such as rats[26-29] and rabbits.[30-32] These studies have made important contributions to the development of strategies for calvarial bone regeneration. However, rodent calvaria are very different from that of humans, and a large animal CSD model is ultimately necessary for enabling clinical translation. Some recent studies have tested how cell-based approaches can support calvarial bone regeneration in full-sized and miniature swine.[26,33-35] However, none of these studies have tested how autologous stem cells combined with a 3D-printed osteoconductive scaffold can support calvarial bone regeneration in such a large CSD (>7.0 cm²) in swine. In developing and testing novel treatment modalities for calvarial defects, the size of the defect matters greatly; large defects are the most challenging cases for achieving successful bone regeneration. Building on our previous study,[24] we therefore sought to establish a calvarial CSD model in swine, and to further investigate how MSCs combined with osteoconductive biomaterials can support calvarial bone regeneration in this model. We selected swine (Yorkshire farm pigs) as a large animal model because their bone morphology and anatomy are similar to those of humans, as are their healing and bone remodeling processes.[33,36] Furthermore, the head of a full-sized farm pig is larger than that of a human, making it possible to create a large CSD similar to those seen in patients in order to mimic clinical conditions faithfully.[37] The establishment of this calvarial bone CSD model in swine will serve as an important platform for future studies to test different biomaterials in combination with stem or progenitor cells in calvarial bone regeneration.

To develop a regenerative therapy for calvarial CSDs that will produce superior outcomes relative to the current standards of care, we used dental pulp-derived mesenchymal stem cells (MSCs) and compared it to BMA, which also contains MSCs, when used in combination with our 3D-printed HA/TCP scaffold. MSCs are ideally suited for tissue regeneration, as they are unique in their ability to self-renew while maintaining their stemness. These cells are multipotent with the capacity to differentiate into chondrocytes, adipocytes, osteocytes, and a variety of other cell types under the right conditions.[38,39] Our previous study has shown that cranial neural crest-derived MSCs as

well as long bone marrow MSCs combined with HA/TCP particles can support bone regeneration.[40] Here we tested the ability of MSCs derived from the cranial neural crest and long BMA to regenerate bone to repair a CSD in a large animal model. Although dental pulp MSCs delivered with HA/TCP particles support calvarial bone regeneration in a CSD, the surface of the regenerated bone is less than ideal, which motivated us to develop a 3D-printed osteoconductive scaffold to achieve a better outcome in calvarial bone regeneration.

The osteoconductive, 3D-printed scaffold we developed for calvarial bone regeneration in a CSD provides a suitable environment that protects the brain during calvarial bone regeneration, promotes osteogenesis and maintains cell viability while holding the cells in place. Although HA/TCP has been used to support bone regeneration, the engineering of our 3D-printed HA/TCP scaffold is an innovative development.[33] Our HA/TCP scaffold is custom-designed based on the CSD. The lattice design and pore size make it easy to load cells during the surgical procedure. The HA/TCP scaffold is biocompatible, osteoconductive, undergoes degradation following bone regeneration, and has the ability to confine cells in place to achieve an aesthetic surface profile of the newly regenerated calvarial bone. It also facilitates seamless integration of the newly regenerated and existing calvarial bone, resulting in biological repair of a calvarial CSD. We have demonstrated that our therapy yields quality cortical bone of sound structure that is well integrated with the native bone, and moreover, that the new tissue is capable of cellular turnover and remodeling.

MSCs are crucial in supporting calvarial bone regeneration.[35,41] In this study, we have shown that HA/TCP alone, heat-inactivated MSCs, and fibroblasts are insufficient to support bone regeneration in the swine calvarial CSD model; live MSCs appear to be required for complete bone regeneration over the time period of our study. Crucially, when delivered on our 3D-printed osteoconductive scaffold, both DPNCCs and BMA were able to regenerate quality bone in the swine calvaria. The bone regenerated using BMA + HA/TCP scaffold appears to have more trabecular structure than bone regenerated using DPNCCs, consistent with our previous findings.[17] Craniofacial bones differ from long bones in that they develop through a process of intramembranous ossification instead of endochondral, and they contain significantly less marrow space than long bones. Owing to the latter quality, the bones of the face and skull are densely cortical, in contrast to the spongy, trabecular quality of long bones. Due to its crucial function of protecting the brain and sensory organs, the strength and quality of regenerated craniofacial bone must be considered carefully. Importantly, our density analysis indicates that the trabecular bone regenerated using BMA when combined with our HA/TCP scaffold is comparable to the native bone in its mechanical properties, suggesting that it would be both dense and strong enough to protect the brain. The capacity of both neural crest- and BMA-derived cells to regenerate cortical bone when combined with our HA/TCP scaffold in the calvaria may indicate environment-dependent differentiation of MSCs. For future clinical practice, either DPNCCs or BMA could be suitable for use with our scaffold to regenerate calvarial bone.

One of the most clinically important aspects of the present work lies in our finding that BMA can support calvarial CSD repair when combined with our 3D-printed scaffold. Using minimally manipulated BMA directly after harvest to support calvarial bone regeneration has several distinct advantages. First, it obviates the need for expansion of the cells, which is costly and time-consuming. Second, it reduces the potential for contamination or loss of stemness of the MSCs due to their expansion in cell culture. Currently, the advantage may lie with BMA over neural crest-derived stem cells for these reasons. However, previous results and the current study indicate that if a source of "off-the-shelf" allogeneic cranial neural crest-derived MSCs were to become available, they could represent an excellent option.

5 | CONCLUSION

In summary, we have established a large animal calvarial CSD model with high preclinical value. Using this model, we have successfully tested a novel approach for skull bone regeneration that combines a 3D-printed osteoconductive scaffold with dental pulp MSCs or BMA. In comparison to the current treatment for patients with CSDs in the skull, our approach will offer patients a safe and effective biological solution to restore skull form and function, and to improve the quality of life for patients.

CONFLICT OF INTEREST
The authors declared no potential conflicts of interest.

AUTHOR CONTRIBUTIONS
Z.M.J. and Y.Y.: conception and design, collection and assembly of data, data analysis and interpretation, manuscript writing; X.L.: conception and design, collection and assembly of data, manuscript writing; T.J.: collection of data, data analysis and interpretation; M.J. and M.U.: conception and design, data interpretation; Y. Chen and Y. Chai: conception and design, data analysis and interpretation, manuscript writing.

DATA AVAILABILITY STATEMENT
The data that supports the findings of this study are available in the main article and supplementary material.

ORCID
Zoe M. Johnson https://orcid.org/0000-0001-7221-361X
Yang Chai https://orcid.org/0000-0003-2477-7247

REFERENCES

1. Badhey A, Kadakia S, Mourad M, Inman J, Ducic Y. Calvarial reconstruction. *Semin Plast Surg*. 2017;31(4):222-226. https://doi.org/10.1055/s-0037-1606557.

2. Aydin S, Kucukyuruk B, Abuzayed B, Aydin S, Sanus GZ. Cranioplasty: review of materials and techniques. *J Neurosci Rural Pract*. 2011;2(2):162-167. https://doi.org/10.4103/0976-3147.83584.

3. Ng ZY, Nawaz I. Computer-designed PEEK implants: a peek into the future of cranioplasty? *J Craniofac Surg*. 2014;25(1):e55-e58. https://doi.org/10.1097/SCS.0b013e3182a2f7b6.

4. Lam S, Kuether J, Fong A, et al. Cranioplasty for large-sized calvarial defects in the pediatric population: a review. *Craniomaxillofac Trauma Reconstr*. 2015 Jun;8(2):159-170. https://doi.org/10.1055/s-0034-1395880.

5. Hill CS, Luoma AM, Wilson SR, et al. Titanium cranioplasty and the prediction of complications. *Br J Neurosurg*. 2012;26(6):832-837. https://doi.org/10.3109/02688697.2012.692839.

6. Garland CB, Pomerantz JH. Regenerative strategies for craniofacial disorders. *Front Physiol*. 2012;3:453. https://doi.org/10.3389/fphys.2012.00453.

7. Fearon JA, Griner D, Ditthakasem K, Herbert M. Autogenous bone reconstruction of large secondary skull defects. *Plast Reconstr Surg*. 2017;139(2):427-438. https://doi.org/10.1097/PRS.0000000000002941.

8. Grant GA, Jolley M, Ellenbogen RG, et al. Failure of autologous bone-assisted cranioplasty following decompressive craniectomy in children and adolescents. *J Neurosurg*. 2004;100(2 suppl pediatrics):163-168. https://doi.org/10.3171/ped.2004.100.2.0163.

9. Jiang Y, Jahagirdar BN, Reinhardt RL, et al. Pluripotency of mesenchymal stem cells derived from adult marrow. *Nature*. 2002;418(6893):41-49. https://doi.org/10.1038/nature00870.

10. Biteau B, Hochmuth CE, Jasper H. Maintaining tissue homeostasis: dynamic control of somatic stem cell activity. *Cell Stem Cell*. 2011;9(5):402-411. https://doi.org/10.1016/j.stem.2011.10.004.

11. Ramesh N, Moratti SC, Dias GJ. Hydroxyapatite-polymer biocomposites for bone regeneration: a review of current trends. *J Biomed Mater Res*. 2018;106(5):2046-2057. https://doi.org/10.1002/jbm.b.33950.

12. Sulaiman SB, Keong TK, Cheng CH, et al. Tricalcium phosphate/hydroxyapatite (TCP-HA) bone scaffold as potential candidate for the formation of tissue engineered bone. *Indian J Med Res*. 2013;137(6):1093-1101.

13. Mauney JR, Volloch V, Kaplan DL. Role of adult mesenchymal stem cells in bone tissue engineering applications: current status and future prospects. *Tissue Eng*. 2005;11(5–6):787-802. https://doi.org/10.1089/ten.2005.11.787.

14. Pepla E, Besharat LK, Palaia G, et al. Nano-hydroxyapatite and its applications in preventive, restorative and regenerative dentistry: a review of literature. *Ann Stomatol (Roma)*. 2014;5(3):108-114.

15. Hubbell J. Biomaterials in tissue engineering. *Nat Biotechnol*. 1995;13:565-576. https://doi.org/10.1038/nbt0695-565.

16. Kang H-W, Lee SJ, Ko IK, Kengla C, Yoo JJ, Atala A. A 3D bioprinting system to produce human-scale tissue constructs with structural integrity. *Nat Biotechnol*. 2016;34(3):312-319.

17. Chung IH, Yamaza T, Zhao H, Choung PH, Shi S, Chai Y. Stem cell property of postmigratory cranial neural crest cells and their utility in alveolar bone regeneration and tooth development. *STEM CELLS*. 2009;27(4):866-877. https://doi.org/10.1002/stem.2.

18. Swindle MM. Bone Marrow Access in Swine. Sinclair Bio Resources; 2009. http://www.sinclairresearch.com/assets/sites/2/Bone-Marrow-Access.pdf. Accessed 2017.

19. Feyen DA, van den Akker F, Noort W, et al. Isolation of pig bone marrow-derived mesenchymal stem cells. *Methods Mol Biol*. 2016;1416:225-232. https://doi.org/10.1007/978-1-4939-3584-0_12.

20. Li X, Yuan Y, Liu L, et al. 3D printing of hydroxyapatite/tricalcium phosphate (HA/TCP) scaffold with hierarchical porous structure for bone regeneration. *Biodes Manuf*. 2019;3(3):15-29. https://doi.org/10.1007/s42242-019-00056-5.

21. Song X, Chen Z, Lei L, et al. Piezoelectric component fabrication using projection Stereolithography of barium Titanate ceramic suspensions. *Rapid Prototyp J*. 2017;23:1.

22. Song X, Chen Y, Lee TW, Wu S, Cheng L. Ceramic fabrication using mask-image-projection-based stereolithography integrated with tape-casting. *SME J Manuf Process*. 2015;20:456-464.

23. Fischer AH, Jacobson KA, Rose J, et al. Hematoxylin and eosin staining of tissue and cell sections. *CSH Protoc*. 2008;2008(5). https://doi.org/10.1101/pdb.prot4986.

24. Park S, Zhao H, Urata M, Chai Y. Sutures Possess Strong Regenerative Capacity for Calvarial Bone Injury. *Stem Cells Dev*. 2016;25(23):1801-1807.

25. Li Y, Chen SK, Li L, et al. Bone defect animal models for testing efficacy of bone substitute biomaterials. *J Orthop Transl*. 2015;3(3):95-104. https://doi.org/10.1016/j.jot.2015.05.002.

26. Mardas N, Kostopoulos L, Karring T. Bone and suture regeneration in calvarial defects by e-PTFE-membranes and demineralized bone matrix and the impact on calvarial growth: an experimental study in the rat. *J Craniofac Surg*. 2002;13(3):453-462.discussion 462-464.

27. Spicer PP, Kretlow JD, Young S, Jansen JA, Kasper FK, Mikos AG. Evaluation of bone regeneration using the rat critical size calvarial defect. *Nat Protoc*. 2012;7(10):1918-1929. https://doi.org/10.1038/nprot.2012.113.

28. Liu Y, Kikuiri T, Akiyama K, et al. Mesenchymal stem cell-based tissue regeneration is governed by recipient T lymphocytes via IFN-γ and TNF-α. *Nat Med*. 2011;17(12):1594-1601. https://doi.org/10.1038/nm.2542.

29. Bae EB, Park KH, Shim JH, et al. Efficacy of rhBMP-2 loaded PCL/β-TCP/bdECM scaffold fabricated by 3D printing technology on bone Regeneration. *BioMed Res Int*. 2018;2018:1-12. http://doi.org/10.1155/2018/2876135.

30. Maliha SG, Lopez CD, Coelho PG, et al. Bone tissue engineering in the growing calvarium using dipyridamole-coated 3D printed bioceramic scaffolds: construct optimization and effects to cranial suture patency. *Plast Reconstr Surg*. 2020;145(2):337e-347e. https://doi.org/10.1097/PRS.0000000000006483.

31. Young S, Bashoura AG, Borden T, et al. Development and characterization of a rabbit alveolar bone nonhealing defect model. *J Biomed Mater Res A*. 2008;86(1):182-194. https://doi.org/10.1002/jbm.a.31639.

32. Shim JH, Jeong J, Won JY, et. al. Porosity effect of 3D-printed polycaprolactone membranes on calvarial defect model for guided bone regeneration. *Biomed Mater*. 2017;13(1):015014. http://doi.org/10.1088/1748-605x/aa9bbc.

33. Rubessa M, Polkoff K, Bionaz M, et al. Use of pig as a model for mesenchymal stem cell therapies for bone regeneration. *Anim Biotechnol*. 2017;28(4):275-287. https://doi.org/10.1080/10495398.2017.1279169.

34. Wehrhan F, Amann K, Molenberg A, Lutz R, Neukam FW, Schlegel KA. PEG matrix enables cell-mediated local BMP-2 gene delivery and increased bone formation in a porcine critical size defect model of craniofacial bone regeneration. *Clin Oral Implants Res*. 2012;23(7):805-813. https://doi.org/10.1111/j.1600-0501.2011.02223.x.

35. Cao Y, Xiong J, Mei S, et al. Aspirin promotes bone marrow mesenchymal stem cell-based calvarial bone regeneration in mini swine. *Stem Cell Res Ther*. 2015;6:210. https://doi.org/10.1186/s13287-015-0200-4.

36. Thorwarth M, Schultze-Mosgau S, Kessler P, Wiltfang J, Schlegel KA. Bone regeneration in osseous defects using a resorbable nanoparticular hydroxyapatite. *J Oral Maxillofac Surg*. 2005;63(11):1626-1633. https://doi.org/10.1016/j.joms.2005.06.010.

37. Weickenmeier J, Kurt M, Ozkaya E, Wintermark M, Pauly KB, Kuhl E. Magnetic resonance elastography of the brain: a comparison between pigs and humans. *J Mech Behav Biomed Mater*. 2018;77:702-710. https://doi.org/10.1016/j.jmbbm.2017.08.029.

38. Langer R, Vacanti J. Advances in tissue engineering. *J Pediatr Surg*. 2016;51(1):8-12. https://doi.org/10.1016/j.jpedsurg.2015.10.022.

39. Mao JJ, Giannobile WV, Helms JA, et al. Craniofacial tissue engineering by stem cells. *J Dent Res*. 2006;85(11):966-979. https://doi.org/10.1177/154405910608501101.

40. Chang S, Hsu Y, Wang YJ, et al. Fabrication of pre-determined shape of bone segment with collagen-hydroxyapatite scaffold and autogenous platelet-rich plasma. *J Mater Sci Mater Med*. 2009;20:23-31. https://doi.org/10.1007/s10856-008-3507-1.

41. Stockmann P, Park J, von Wilmowsky C, et al. Guided bone regeneration in pig calvarial bone defects using autologous mesenchymal stem/progenitor cells - a comparison of different tissue sources. *J Craniomaxillofac Surg*. 2012;40(4):310-320. https://doi.org/10.1016/j.jcms.2011.05.004.

SUPPORTING INFORMATION

Additional supporting information may be found online in the Supporting Information section at the end of this article.